PHYSICAL REVIEW B **89**, 020408(R) (2014)

# Renormalization group analysis of competing quantum phases in the $J_1$-$J_2$ Heisenberg model on the kagome lattice

Raik Suttner,[1] Christian Platt,[1] Johannes Reuther,[2] and Ronny Thomale[1]
[1]*Institute for Theoretical Physics and Astrophysics, University of Würzburg, D-97074 Würzburg, Germany*
[2]*Department of Physics, California Institute of Technology, Pasadena, California 91125, USA*
(Received 9 March 2013; revised manuscript received 24 November 2013; published 21 January 2014)

Recent discoveries in neutron scattering experiments for Kapellasite and Herbertsmithite as well as theoretical calculations of possible spin liquid phases have revived interest in magnetic phenomena on the kagome lattice. We study the quantum phase diagram of the $S = 1/2$ Heisenberg kagome model as a function of nearest neighbor coupling $J_1$ and second neighbor coupling $J_2$. Employing the pseudofermion functional renormalization group (PFFRG), we find four types of magnetic quantum order ($\mathbf{q} = 0$ order, cuboc order,ferromagnetic order, and $\sqrt{3} \times \sqrt{3}$ order) as well as extended magnetically disordered regions by which we specify the possible parameter regime for Kapellasite. In the disordered regime $\frac{J_2}{J_1} \ll 1$, the flatness of the magnetic susceptibility at the zone boundary which is observed for Herbertsmithite can be reconciled with the presence of small $J_2 > 0$ coupling. In particular, we analyze the dimer susceptibilities related to different valence-bond crystal (VBC) patterns, which are strongly inhomogeneous, indicating the rejection of VBC order in the RG flow.

DOI: 10.1103/PhysRevB.89.020408 PACS number(s): 75.10.Jm, 75.10.Kt

*Introduction*. Frustrated magnetism is a focus of contemporary research in condensed matter physics, combining a plethora of experimental scenarios and diverse theoretical approaches to describe them. One of the most fascinating challenges of the field has been to investigate and understand the interplay of magnetic quantum order and disorder on the kagome lattice. A major reason why this lattice of corner-sharing triangles yields such a complicated structure of quantum phases is already evident from the classical kagome Heisenberg model (KHM): As a function of nearest neighbor and next nearest neighbor Heisenberg couplings $J_1$ and $J_2$, many different magnetic orders are present [1,2], where an infinite number of degenerate ground states can be found [3]. From a theoretical perspective, not many rigorous results about the quantum phase diagram are known so far. Advanced mean field theories have provided important guidance as to what type of ordered and disordered quantum phases could possibly be found [4–10], but cannot give unambiguous information about which phase will eventually be stabilized in the microscopic model. A peculiar feature of the KHM which has been known since early exact numerical calculations of finite size clusters [11] is the large amount of singlet states at low energy. This suggests an overabundance of competing quantum-disordered phases and is probably one of the main reasons why the interpretation of the present results for the $J_1$ KHM from microscopic numerical approaches is not yet fully settled [12–17].

Transferring our fragile theoretical knowledge to experimental scenarios is even more challenging. The Herbertsmithite compound $ZnCu_3(OH)_6Cl_2$ is one of the rare, properly investigated material realizations of a $S = 1/2$ kagome spin model, which is supposedly dominated by the $J_1$ term. Early investigations from neutrons [18] and muon spin rotation ($\mu$SR) [19] have already indicated its unconventional frustrated magnetic properties, exhibiting no sign of magnetic order down to a few mK. While there is no indication for a magnetic spin gap, it is likely that this does not hint at a key property of a possible KHM description, but might be due to Dzyaloshinskii-Moriya (DM) effects and impurities which further complicate the picture (see, e.g., Refs. [18–23]). The latest detailed neutron scattering experiments resolve a flat magnetic susceptibility profile [24,25], which allows for an interpretation along spin fractionalization as known, e.g., from spinon continua in the spin structure factor of quasi-one-dimensional systems [26]. Recently, neutron and $\mu$SR experiments on Kapellasite, $Cu_3Zn(OH)_6Cl_2$, of which Herbertsmithite is a polymorph, have found indications for cuboc short-range correlations [27]. This is an exciting discovery, as electronic structure calculations find dominant *antiferromagnetic* $J_1$ coupling and hence a similar regime as Herbertsmithite [28]. From where classical cuboc order emerges, however, this suggests the presence of *ferromagnetic* $J_1$ and antiferromagnetic $J_2$ in Kapellasite [29].

In this Rapid Communication, we develop a pseudofermion functional renormalization group (PFFRG) perspective on the $J_1$-$J_2$ kagome Heisenberg model which is ideally suited to treat magnetic order and disorder tendencies on an unbiased footing [30–35]. Our objectives are twofold. First, we obtain a detailed understanding of the $J_1$-$J_2$ quantum phase diagram, including all magnetically ordered and disordered regimes as well as the associated phase transitions. In particular, in light of recent findings for compounds such as Kapellasite, we allow both $J_1$ and $J_2$ couplings to be ferromagnetic and antiferromagnetic. Aside from ferromagnetic, cuboc, $\sqrt{3} \times \sqrt{3}$, and $\mathbf{q} = 0$ order, we find magnetically disordered regimes located around $(J_1, J_2) \sim (1,0)$, $(J_1, J_2) \sim (0,1)$, and possibly a nonmagnetic phase separating the cuboc from the ferromagnetic domain (Fig. 1). Second, we specifically investigate the $J_1$ KHM disordered regime which is supposed to relate to the Herbertsmithite scenario. Due to the large system sizes of up to 317 sites which are reached by PFFRG, we obtain accurate resolution of the momentum-resolved static magnetic susceptibility. Aside from short-range correlations, we observe a broad spectral distribution which becomes flat at the magnetic zone boundary for $J_2/J_1 \sim 0.017$ (Fig. 2). This profile is similar to what is observed in recent neutron

 

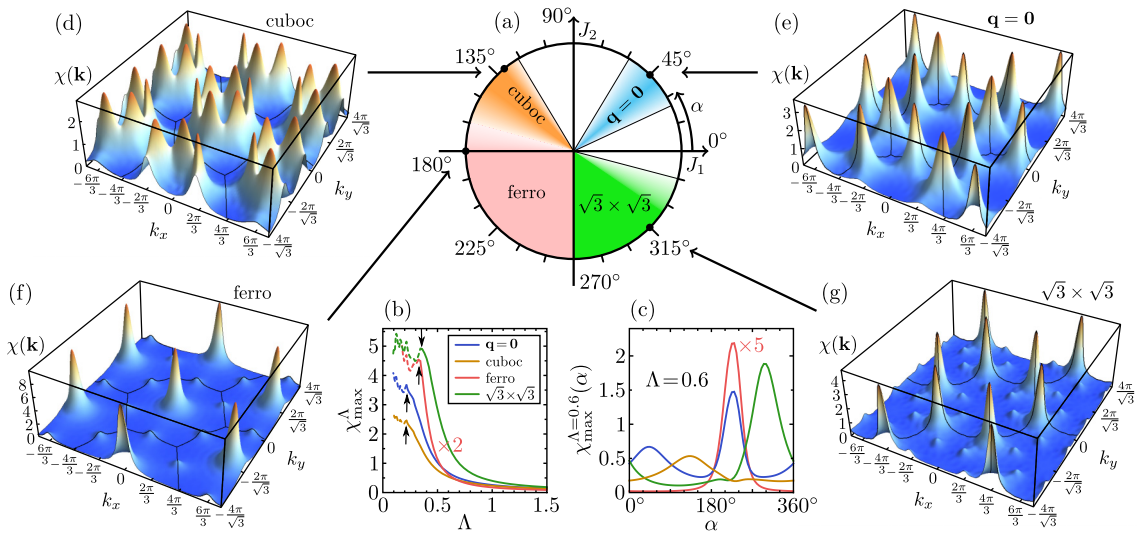


FIG. 1. (Color online) (a) Quantum phase diagram of the $J_1$-$J_2$ kagome Heisenberg model. Colored regions correspond to the magnetically ordered phases $\mathbf{q}=0$, cuboc, ferromagnetic, and $\sqrt{3}\times\sqrt{3}$ order, while white regimes are nonmagnetic. Faint areas near the phase transitions (e.g., between the cuboc and the ferromagnetic phase) are regions of significant numerical uncertainty. (b) Flow of the susceptibilities at the ordering vectors of the four ordered regimes. Arrows indicate the instability features. The curves for $\mathbf{q}=0$, cuboc, ferromagnetic, and $\sqrt{3}\times\sqrt{3}$ order are given for $\alpha = 45^\circ$, $130^\circ$, $180^\circ$, and $315^\circ$, respectively (black dots in the phase diagram). (c) Susceptibilities at the ordering vectors of the ordered phases as a function of $\alpha$ at constant $\Lambda = 0.6$, well above the instability features. Ordered regimes occur in the vicinity of the maxima of these curves. (d)–(g) show the susceptibility profiles for all types of orders (at the points indicated in the phase diagram) at the instability breakdown.

measurements [25]. Furthermore, we compute the dimer susceptibilities for different pattern candidates. While local pinwheel correlations tend to get enhanced by the RG flow, long-range valence-bond crystal (VBC) orders are rejected, as seen by a strongly inhomogeneous pattern response (Fig. 3). This suggests that the initial RG bias for VBC flows away towards a random valence-bond (RVB) liquid type state, which is consistent with spin liquid proposals for the KHM.

*Model*. The Hamiltonian of the $J_1$-$J_2$ kagome Heisenberg model (KHM) is given by

$$H_{\mathrm{KHM}} = J_1 \sum_{\langle ij\rangle} \mathbf{S}_i \mathbf{S}_j + J_2 \sum_{\langle\langle ij\rangle\rangle} \mathbf{S}_i \mathbf{S}_j, \qquad (1)$$

where $\langle ij\rangle$ and $\langle\langle ij\rangle\rangle$ denote nearest neighbor and second neighbor pairs, respectively. We parametrize the couplings by $J_1 = J\cos\alpha$ and $J_2 = J\sin\alpha$, which enables us to characterize each point in parameter space by a single angle $\alpha$ (Fig. 1), with $0 \leqslant \alpha < 2\pi$. (All energies are given in units of $J$ in the following.) For $\alpha = 90^\circ$, the system decouples into three independent kagome lattices, which implies that the system at this point has the same physical properties as at $\alpha = 0$. For its classical counterpart [29], the $J_1$-$J_2$ KHM exhibits four types of magnetic order: (i) the planar $\mathbf{q}=0$ Néel state with a three-site unit cell which appears for purely antiferromagnetic interactions at $0^\circ < \alpha < 90^\circ$, (ii) the nonplanar cuboc state with a 12-site unit cell located at $90^\circ < \alpha < 161.6^\circ$, (iii) a ferromagnetic phase at $161.6^\circ < \alpha < 270^\circ$, and (iv) the planar $\sqrt{3}\times\sqrt{3}$ Néel state with a nine-site unit cell in the region $270^\circ < \alpha < 360^\circ$ (the phases are also found in the quantum phase diagram, Fig. 1). These types of order correspond to

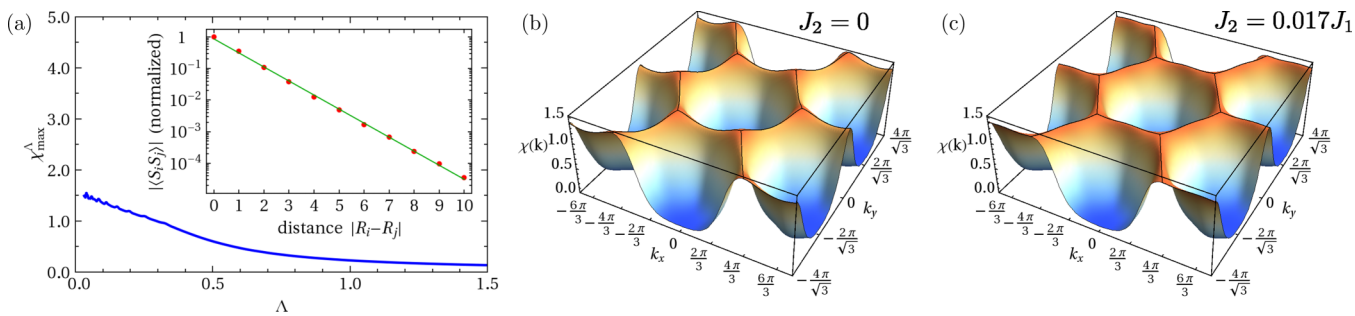


FIG. 2. (Color online) Nonmagnetic phase for $|\frac{J_2}{J_1}| \ll 1$: (a) $\Lambda$ flow of the largest $\boldsymbol{k}$ component of the magnetic susceptibility for $\alpha = 0$. The flow behavior is smooth to $\Lambda = 0$. (Small oscillations below $\Lambda \approx 0.3$ are due the frequency discretization.) (b), (c) $\boldsymbol{k}$-space resolved susceptibility at $\Lambda = 0$. Small maxima can be seen at the $K$ points of the second Brillouin zone for $J_2 = 0$ in (b). These maxima vanish for at $J_2 = 0.017J_1$ in (c), with a strong resemblance to Ref. [25].

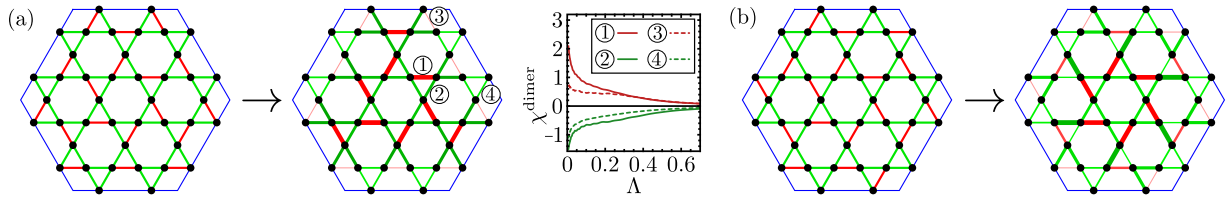


FIG. 3. (Color online) Dimer configuration for (a) the HVBC [40] and (b) the modified HVBC before (left) and after (right) the RG flow. Red lines correspond to strengthened and green lines to weakened bonds, where the thickness of the lines encodes the magnitude of the response. The blue lines mark the unit cell of the pattern. (a) Local pinwheel structure gets enhanced during the flow, while the outer bond responses are inhomogeneous, indicating the rejection of long-range order. Representative flows of the response on selected bonds are also plotted. (b) A modified HVBC with 60° rotation symmetry shows similar features as (a).

different ordering-peak positions in the second Brillouin zone [36]. For real-space illustrations of the different orders, we refer to the Refs. [29,37].

*Pseudofermion functional renormalization group*. The PFFRG approach [30–33,36], which we employ to obtain the quantum phase diagram displayed in Fig. 1, starts by reformulating the spin Hamiltonian in terms of a pseudofermion representation of the spin-1/2 operators $S^\mu = 1/2 \sum_{\alpha\beta} f^\dagger_\alpha \sigma^\mu_{\alpha\beta} f_\beta$ $(\alpha,\beta = \uparrow,\downarrow,\ \mu = x,y,z)$ with fermionic operators $f_\uparrow$ and $f_\downarrow$ and Pauli matrices $\sigma^\mu$. This allows us to apply Wick's theorem, leading to standard Feynman many-body techniques. We further introduce an infrared frequency cutoff $\Lambda$ in the fermionic propagator. The FRG ansatz then formulates equations for the evolution of all $m$-particle vertex functions [38] under the flow of $\Lambda$. To reduce the infinite hierarchy of coupled equations to a closed set, the PFFRG only includes two-particle reducible two-loop contributions [39], which still assures a sufficient backfeeding of the self-energy corrections to the two-particle vertex evolution. A crucial advantage of the PFFRG as compared to Abrikosov-type spin–random phase approximation (RPA) methods is that the summations include vertex corrections between all interaction channels, i.e., the two-particle vertex includes graphs that favor magnetic order and those that favor disorder in such a way that it treats both tendencies on an equal footing. Solving the PFFRG equations requires (i) to discretize the frequency dependencies and (ii) to limit the spatial dependence to a finite cluster. In our calculations, the latter typically includes a correlation area (cluster size) of 317 lattice sites. The onset of spontaneous long-range order is signaled by a sudden breakdown of the smooth RG flow, while the existence of a stable solution indicates the absence of long-range order [30,31]. From the effective low-energy two-particle vertex, we obtain the spin susceptibility with a high momentum resolution (Figs. 1 and 2) and, in the case of a magnetically disordered regime, track possible VBC orders [32] by computing the response functions to different dimer patterns (Fig. 3).

*Quantum phase diagram*. As shown in Fig. 1(a), we find ferromagnetic, cuboc, $\mathbf{q} = 0$, and $\sqrt{3} \times \sqrt{3}$ Néel order in the quantum $J_1$-$J_2$ KHM. Figure 1(b) shows the RG flow in the four magnetically ordered phases. Clear instability breakdowns as resolved by strong kinks are seen in the ferromagnetic and in the $\sqrt{3} \times \sqrt{3}$ Néel phase. In the $\mathbf{q} = 0$ Néel phase and in the cuboc phase, however, the instability features are less pronounced, which is consistent with a small magnetization. We conclude that disorder fluctuations are still important in these regions. The sequence of different ordering tendencies as a function of $\alpha$ is also indicated in Fig. 1(c), showing the susceptibility at constant $\Lambda = 0.6$. Figures 1(d)–1(g) illustrate susceptibility profiles of the magnetically ordered phases (the plots are taken for the cutoff value $\Lambda_c$ at the instability breakdown). They exhibit distinct peak structures as expected for the different orders [36]. Note that for the ferromagnetic and the $\sqrt{3} \times \sqrt{3}$ Néel phase, the PFFRG also accurately resolves the expected subdominant peaks.

Due to quantum fluctuations, magnetically disordered phases complement the ordered phases in the $J_1$-$J_2$ KHM quantum phase diagram. We find a nonmagnetic region for $338° \lesssim \alpha \lesssim 35°$ (Fig. 1). A similar nonmagnetic phase is found for $56° \lesssim \alpha \lesssim 124°$. In addition, we find indications for a small disordered phase at $\alpha \approx 161°$. Enhanced uncertainties near the phase boundary between the cuboc and the ferromagnetic phase, however, make it hard to resolve the range of this phase.

For comparison of our phase diagram with related works, we emphasize that the quantum phase diagram of the KHM still needs to be calculated in the full $\alpha$-parameter space. Reference [29] finds the phase transition between the cuboc ordered phase and the $J_2$-dominated nonmagnetic phase at $\alpha = 108°$, i.e., at somewhat smaller $J_1$ as compared to our results. Exact diagonalization studies [41] locate the transition between the $\sqrt{3} \times \sqrt{3}$ order and the $J_1$-dominated nonmagnetic phase at $\alpha \lesssim 333°$, in approximate agreement with our findings. Furthermore, the asymmetric location of the $J_1$-dominated nonmagnetic phase with respect to negative and positive $J_2$ is also reported in Ref. [42].

The comparably small regime of unambiguous cuboc order is an important piece of information in light of the recent experimental findings for Kapellasite [27]. Our results confirm that the only way to accomplish such a phase in the quantum $J_1$-$J_2$ KHM is the existence of a ferromagnetic $J_1$ and a considerable antiferromagnetic $J_2$, while even longer-range Heisenberg couplings might additionally be important [43]. In particular, we find the cuboc phase in a regime with enhanced quantum fluctuations, suggesting that comparably small changes of system parameters should induce a significant change in $T_N$ and the general magnetic susceptibility profile. The PFFRG is ideally suited to track the evolution of the susceptibility peaks in the cuboc domain, which we defer to a later point.

*Disordered phase for* $|\frac{J_2}{J_1}| \ll 1$. The $J_1$ KHM ($\alpha = 0$) has been frequently studied in the literature, and it is supposed

to be close to the parameter regime where Herbertsmithite is located. There, we find that the RG flow remains stable in the entire flow regime, such that the RG equations can be smoothly integrated down to $\Lambda = 0$. Figure 2(a) depicts the largest susceptibility component (i.e., the one at the $K$ points of the second Brillouin zone). No sign of any instability breakdown is seen during the flow, which is a signature for a nonmagnetic ground state. This property along with the indication for a spin gap is also reflected in the spin-spin correlations [see the inset of Fig. 2(a)]. Our data show an almost perfect exponential decay of the correlations in real space, from which we determine a small correlation length of only $\xi = 0.98$ lattice constants. This is in agreement with density matrix renormalization group (DMRG) calculations [12,13,15] which find correlation lengths between 0.8 and 1.5 lattice spacings. The full $\boldsymbol{k}$-space resolved susceptibility in Fig. 2(b) reveals further information about the magnetic properties at $\alpha = 0$. The susceptibility is mainly concentrated at the boundary of the second Brillouin zone and is almost constant along the whole edge. Fluctuations at such large $\boldsymbol{k}$ are consistent with the small correlation length. The susceptibility along the edge shows only small maxima at the $K$ points, which have also been found in DMRG calculations [15]. (Comparing to exact diagonalization results of smaller size, this emphasizes similarities, but also discrepancies, due to finite torus loop resonance artifacts for small tori [44].) As a result, subleading $\sqrt{3} \times \sqrt{3}$ fluctuations are preferred as compared to other fluctuations at the Brillouin zone boundary. Most of the discovered features such as a broad susceptibility profile are shared by neutron scattering susceptibility measurements in Herbertsmithites, and might hint at spin fractionalization which can emerge in various spin liquid scenarios [25]. One major discrepancy, however, is the lack of any maxima at the $K$ points in the actual measurements. By increasing $J_2$, we discover that the previous maxima at $\alpha = 0$ vanish and look similar to the experimental finding: Figure 2(c) shows the spin susceptibility at $J_2/J_1 = 0.017$, indicating that the absence of the boundary peaks in Herbertsmithite can be explained by the presence of a small, but finite, $J_2 > 0$ coupling.

The natural competitor for a spin liquid in such a magnetically disordered phase is VBC order. For $\alpha = 0$, we have considered generalized susceptibilities which measure the propensity of the system to form a specific VBC. As has been shown by dimer expansions [40], the honeycomb VBC (HVBC) [Fig. 3(a)] is the most promising dimerization pattern for the $J_1$ KHM. It is a longstanding question whether or not the ground state of this system is a HVBC. In order to calculate valence-bond susceptibilities for such dimer coverings within our RG approach, we add a small perturbation $H_{\mathrm{D}}$ to the model in (1) which increases ($J_1 \to J_1 + \delta$) or decreases ($J_1 \to J_1 - \delta$) the couplings on the nearest neighbor bonds, according to the dimer pattern. If the system supports the dimer pattern, the strong bonds become stronger and the weak bonds become weaker during the flow [36].

The RG flow of the HVBC pattern is depicted in Fig. 3(a). The left picture denotes the modified bond strengths at the start of the RG flow. The right picture shows the bond strengths after the flow at $\Lambda = 0$. As is clearly visible, the pinwheel bonds around the rotation center of the HVBC structure are strongly and homogeneously enhanced. This has been noticed before, as the pinwheel is an approximate local eigenstate for the KHM [40]. On the other hand, as also reported in Ref. [13], the "perfect hexagons" (i.e., the hexagons with three dimer bonds along its edges, located at the corners of the so-defined VBC unit cell in Fig. 3) is a source of small response, which in total leads to very inhomogeneous valence-bond susceptibilities. As a further attempt, we have investigated a modified HVBC pattern where the pinwheel structure stays unchanged, but the arrangement of the outer bonds is modified [Fig. 3(b)]. The results we obtain show the same magnitudes and inhomogeneities of dimer responses as for the HVBC. Keeping the pinwheel structure, we have also investigated further possible VBC patterns [36]. The unified picture emerging from our studies is that while the pinwheel structures are reasonable guesses for the local correlation profile in the KHM, we do not find any sign of long-range VBC order, as all VBCs we have tested exhibit similar response patterns. More so, the findings of many competing VBC pattern candidates frustrating each other resemble the short-range RVB liquid hypothesis, which can seed the emergence of spin liquids [45].

To summarize, we have obtained the quantum phase diagram of the $J_1$-$J_2$ KHM and have investigated its magnetic and nonmagnetic phases. In light of recent experiments on Kapellasite, it will be interesting to further investigate the interplay of order and disorder in the cuboc order regime. Furthermore, we have provided model evidence for explaining the features of the susceptibility measurements in Herbertsmithite, and specifically link the absence of boundary susceptibility enhancements to the existence of small but finite $J_2$ coupling. We have also found indications for RVB liquid physics in the $J_1$ KHM, rendering the related Herbertsmithite a prime candidate for observing a spin liquid phase in nature.

*Acknowledgments*. R.T. thanks A. C. Potter, D. Mross, C. Lhuillier, A. Läuchli, P. A. Lee, F. Mila, and all participants of the KITP workshop "Frustrated Magnetism and Quantum Spin Liquids: From Theory and Models to Experiments." C.P. and R.T. are supported by SPP 1458. J.R. acknowledges support from the Deutsche Akademie der Naturforscher Leopoldina through Grant No. LPDS 2011-14.

[1] A. B. Harris, C. Kallin, and A. J. Berlinsky, Phys. Rev. B **45**, 2899 (1992).
[2] M. Spenke and S. Guertler, Phys. Rev. B **86**, 054440 (2012).
[3] J. T. Chalker, P. C. W. Holdsworth, and E. F. Shender, Phys. Rev. Lett. **68**, 855 (1992).
[4] P. W. Anderson, Science **235**, 1196 (1987).
[5] J. B. Marston and C. Zeng, J. Appl. Phys. **69**, 5962 (1991).
[6] X. G. Wen, Phys. Rev. B **44**, 2664 (1991).
[7] S. Sachdev, Phys. Rev. B **45**, 12377 (1992).
[8] M. B. Hastings, Phys. Rev. B **63**, 014413 (2000).
[9] Y. Ran, M. Hermele, P. A. Lee, and X.-G. Wen, Phys. Rev. Lett. **98**, 117205 (2007).

[10] L. Messio, B. Bernu, and C. Lhuillier, Phys. Rev. Lett. **108**, 207204 (2012).
[11] C. Waldtmann, H. U. Everts, B. Bernu, C. Lhuillier, P. Sindzingre, P. Lecheminant, and L. Pierre, Eur. Phys. J. B **2**, 501 (1998).
[12] H. C. Jiang, Z. Y. Weng, and D. N. Sheng, Phys. Rev. Lett. **101**, 117203 (2008).
[13] S. Yan, D. A. Huse, and S. R. White, Science **332**, 1173 (2011).
[14] T. Tay and O. I. Motrunich, Phys. Rev. B **84**, 020404 (2011).
[15] S. Depenbrock, I. P. McCulloch, and U. Schollwöck, Phys. Rev. Lett. **109**, 067201 (2012).
[16] H.-C. Jiang, Z. Wang, and L. Balents, Nat. Phys. **8**, 902 (2012).
[17] Y. Iqbal, F. Becca, S. Sorella, and D. Poilblanc, Phys. Rev. B **87**, 060405(R) (2013).
[18] J. S. Helton, K. Matan, M. P. Shores, E. A. Nytko, B. M. Bartlett, Y. Yoshida, Y. Takano, A. Suslov, Y. Qiu, J.-H. Chung, D. G. Nocera, and Y. S. Lee, Phys. Rev. Lett. **98**, 107204 (2007).
[19] P. Mendels, F. Bert, M. A. de Vries, A. Olariu, A. Harrison, F. Duc, J. C. Trombe, J. S. Lord, A. Amato, and C. Baines, Phys. Rev. Lett. **98**, 077204 (2007).
[20] M. Elhajal, B. Canals, and C. Lacroix, Phys. Rev. B **66**, 014422 (2002).
[21] M. A. de Vries, K. V. Kamenev, W. A. Kockelmann, J. Sanchez-Benitez, and A. Harrison, Phys. Rev. Lett. **100**, 157205 (2008).
[22] J. S. Helton, K. Matan, M. P. Shores, E. A. Nytko, B. M. Bartlett, Y. Qiu, D. G. Nocera, and Y. S. Lee, Phys. Rev. Lett. **104**, 147201 (2010).
[23] T. Han, S. Chu, and Y. S. Lee, Phys. Rev. Lett. **108**, 157202 (2012).
[24] D. Wulferding, P. Lemmens, P. Scheib, J. Röder, P. Mendels, S. Chu, T. Han, and Y. S. Lee, Phys. Rev. B **82**, 144412 (2010).
[25] T.-H. Han, J. S. Helton, S. Chu, D. G. Nocera, J. A. Rodriguez-Rivera, C. Broholm, and Y. S. Lee, Nature (London) **492**, 406 (2012).
[26] R. Coldea, D. A. Tennant, and Z. Tylczynski, Phys. Rev. B **68**, 134424 (2003).
[27] B. Fåk, E. Kermarrec, L. Messio, B. Bernu, C. Lhuillier, F. Bert, P. Mendels, B. Koteswararao, F. Bouquet, J. Ollivier, A. D. Hillier, A. Amato, R. H. Colman, and A. S. Wills, Phys. Rev. Lett. **109**, 037208 (2012).
[28] O. Janson, J. Richter, and H. Rosner, Phys. Rev. Lett. **101**, 106403 (2008).
[29] J.-C. Domenge, P. Sindzingre, C. Lhuillier, and L. Pierre, Phys. Rev. B **72**, 024433 (2005).
[30] J. Reuther and P. Wölfle, Phys. Rev. B **81**, 144410 (2010).
[31] J. Reuther and R. Thomale, Phys. Rev. B **83**, 024402 (2011).
[32] J. Reuther, D. A. Abanin, and R. Thomale, Phys. Rev. B **84**, 014417 (2011).
[33] J. Reuther, R. Thomale, and S. Trebst, Phys. Rev. B **84**, 100406 (2011).
[34] S. Göttel, S. Andergassen, C. Honerkamp, D. Schuricht, and S. Wessel, Phys. Rev. B **85**, 214406 (2012).
[35] J. Reuther, R. Thomale, and S. Rachel, Phys. Rev. B **86**, 155127 (2012).
[36] See Supplemental Material at http://link.aps.org/supplemental/10.1103/PhysRevB.89.020408 for further details.
[37] L. Messio, C. Lhuillier, and G. Misguich, Phys. Rev. B **83**, 184401 (2011).
[38] W. Metzner, M. Salmhofer, C. Honerkamp, V. Meden, and K. Schönhammer, Rev. Mod. Phys. **84**, 299 (2012).
[39] A. A. Katanin, Phys. Rev. B **70**, 115109 (2004).
[40] R. R. P. Singh and D. A. Huse, Phys. Rev. B **76**, 180407 (2007).
[41] P. Lecheminant, B. Bernu, C. Lhuillier, L. Pierre, and P. Sindzingre, Phys. Rev. B **56**, 2521 (1997).
[42] S. R. White, Bull. Am. Phys. Soc. **57**, MAR.L19.1 (2012), http://meetings.aps.org/link/BAPS.2012.MAR.L19.1.
[43] B. Bernu, C. Lhuillier, E. Kermarrec, F. Bert, P. Mendels, R. H. Colman, and A. S. Wills, Phys. Rev. B **87**, 155107 (2013).
[44] A. Läuchli and C. Lhuillier, arXiv:0901.1065.
[45] S. A. Kivelson, D. S. Rokhsar, and J. P. Sethna, Phys. Rev. B **35**, 8865 (1987).